October 2001

ELSEVIER

Materials Letters 51 (2001) 101–107

MATERIALS LETTERS

www.elsevier.com/locate/matlet

Liquid phase benzene hydrogenation to cyclohexane over modified Ni–P amorphous catalysts

Hexing Li *, Yeping Xu

Department of Chemistry, Shanghai Normal University, Shanghai 200234, PR China

Received 14 November 2000; accepted 18 December 2000

Abstract

Four kinds of Ni–P amorphous catalysts, ultrafine Ni–P, Ni–P/SiO_2, Ni–W–P/SiO_2 and Raney Ni–P, were prepared by either the rapid quenching technique, following the alkali leaching, or the chemical reduction with NaH_2PO_2. During the liquid phase hydrogenation of benzene, all these catalysts exhibited higher TOF values than Raney Ni catalyst, owing to their unique amorphous structure. Except for the ultrafine Ni–P, which had extremely low surface active area, all the other Ni–P catalysts also exhibited higher activity per gram Ni than Raney Ni. The crystallization of the Ni–P amorphous catalysts at high temperature caused a considerable decrease in their activities. According to various characterizations, the relationship between catalytic activity and the structure of the as-prepared Ni–P catalysts was briefly discussed. © 2001 Published by Elsevier Science B.V.

Keywords: Ni–P amorphous catalysts; Hydrogenation; Benzene; Cyclohexane; Crystallization; Promoting effect

1. Introduction

Hydrogenation of benzene to prepare cyclohexane has been known to be an important industrial process [1], during which Raney Ni catalysts are most frequently employed [2,3]. Due to the high stability of the aromatic rings, many attempts have been made to develop more active catalysts for the benzene hydrogenation, among which the amorphous alloys represent a new generation of hydrogenation catalysts due to their excellent activity, better selectivity and strong sulfur resistance [4]. In industry, the amorphous alloys are mainly prepared in the form of ribbons by the rapid quenching technique [5–7], which seem nearly impossible to be used as practical catalysts due to the extremely low surface area (ca. 1.0 m^2/g) and poor thermal stability. Recently, the amorphous alloy catalysts prepared by chemical reduction have caused much attention, since these catalysts could be prepared in the form of ultrafine particles in a simple procedure. By this method, it is also very convenient to modify the amorphous catalyst with an additional transitional metal and to deposit the ultrafine amorphous alloy particles onto a suitable support. Many systematic studies have been made on surface states, chemisorptive properties and catalytic properties of metal–B amorphous catalysts [8–10], but quite limited work has been done on the metal–P amorphous catalysts [11–14]. In the present paper, several new

* Corresponding author. Tel.: +86-21-64322272; fax: +86-21-64322150.

E-mail address: HeXing-Li@shtu.edu.cn (H. Li).

00167-577X/01/$ - see front matter © 2001 Published by Elsevier Science B.V.
PII: S0167-577X(01)00273-7

kinds of Ni–P amorphous catalysts, such as a skeletal Ni–P amorphous catalyst, an ultrafine Ni–P amorphous catalyst, the silica-supported Ni–P amorphous catalysts with or without W-dopant, were prepared via different methods. During the liquid phase, benzene hydrogenation to cyclohexane, these catalysts exhibited much higher activity than Raney Ni, showing the potential application in industrial processes.

2. Experimental

2.1. Catalyst preparation

Four kinds of Ni–P amorphous catalysts were prepared by the following methods: the ultrafine Ni–P amorphous catalyst was prepared by direct reduction of $NiCl_2$ with NaH_2PO_2 in aqueous solution at 363 K, as described elsewhere [9]; the Ni–P amorphous catalyst deposited on a silica support ($Ni–P/SiO_2$, Ni loading = 11.5 wt%) was prepared by an electroless plating over 1.0 g SiO_2 (40 ~ 60 mesh, 185 m^2/g BET surface area), in 100 ml aqueous solution containing 1.0 g $NaH_2PO_2 \cdot H_2O$, 1.0 g $NiCl_2 \cdot 6H_2O$, 1.0 g NaOAc, 1.0 g $Na_3C_6H_5O_7 \cdot 2H_2O$ (sodium citrate) and 0.05 wt.% gelatin as a dispersing agent. The plating reaction was performed at 363 K with vigorous stirring until the evolution of a gas had ceased, usually within 2 h. The resulting black solid was washed thoroughly with distilled H_2O until free from Cl^- and K^+ ions. Then, it was further washed with absolute alcohol (EtOH) and finally, dried at 423 K in N_2 to increase the interaction between Ni–P alloy and the silica support; The W-doped SiO_2-supported Ni–P amorphous catalyst ($Ni–W–P/SiO_2$, Ni loading = 11.2 wt.%, W/Ni molar ratio = 1.5%) was prepared in the similar way to that of $Ni–P/SiO_2$ amorphous catalyst, by adding desired amount of Na_2WO_4 in the plating solution; the skeletal Ni–P amorphous catalyst (denoted as Raney Ni–P amorphous catalyst due to its similar structure to that of Raney Ni) was prepared by alkali leaching an Ni–Al–P amorphous alloy (48.2%wt Ni, 48.7%wt Al and 3.1%wt P), obtained by the rapid quenching technique from the melting solution containing Ni, Al and P. The optimum leaching conditions were determined as follows: 6.0 g Ni–Al–P, 60-ml 6.0 M NaOH, leaching at 343 K for 6.0 h.

Raney Ni was obtained by alkali leaching of a commercially available Ni–Al alloy under the same conditions as used in the Raney Ni–P preparation.

2.2. Catalyst characterization

The composition and the Ni loading of the as-prepared catalysts were analyzed by ICP. The surface active area (S_{act}) was determined by hydrogen chemisorption using a dynamic pulse method, assuming H/Ni(s) = 1 and a surface area of 6.5×10^{-20} m^2 per Ni atom [15]. Amorphous structure and its alteration during heating pretreatment were determined by X-ray diffraction (XRD, Rigaku Dmax-3C with Cu Kα radiation) and extended X-ray absorption fine structure (EXAFS, BL-10B), carried out in the National Laboratory of High Energy Physics (KEK, Tsukuba, Japan). The thermal stability was determined by differential scanning calorimetry (DSC, Perkin–Elmer, heating rate = 10 K/min). The surface morphology and the particle size were determined by both the scanning electron micrograph (SEM, JSM-840) and the transmission electron micrograph (TEM, Hitachi H 600). The surface electronic states were determined by the X-ray photoelectron spectroscopy (XPS, Perkin–Elmer PH I 5000C). All binding energy values were calibrated by using the value of contaminant carbon (C_{1s} = 284.6 eV) as a reference.

2.3. Activity test

The catalytic activities of the as-prepared catalysts were measured during the benzene hydrogenation in liquid phase at 373 K temperature and 1.0 MPa hydrogen pressure. The hydrogenation was carried in an autoclave containing 1.0 g catalyst, 10 ml benzene and 40 ml alcohol. The reaction mixture was stirred vigorously at 1200 rpm to eliminate the diffusion effects. Initial hydrogenation activity was determined by monitoring the drop of the pressure with the time, which was then turned to be the H_2 uptake rate per gram Ni (R_{H_2} = mmol/h g Ni). Each hydrogenation lasted for 4.0 h. The reaction products were analyzed by gas chromatography with TD detector to obtain the conversion of benzene and the selectivity

to cyclohexane. Reproducibility of the activity test was better than 5%. In addition, TOF values were calculated according to the following equation:

$$\mathrm{TOF} = \left[(V \times d/M) \times C \times 6.02 \times 10^{23} \times S\right] /N \times t,$$

where V is the volume of benzene used in the hydrogenation; d is the density of benzene; M is the molecular mass of benzene; C is the benzene conversion; S is the selectivity to cyclohexane. Under present reaction conditions, $S = 100\%$; N is the number of surface active Ni atoms determined by H_2 chemisorption, t is the reaction time; and 6.02×10^{23} is Avogadro's number. The unit of TOF is per second (s^{-1}).

3. Results and discussion

TEM confirmed that the unsupported Ni–P sample was present in spherical ultrafine particles with the size ranging from 0.5 to 1.2 μm, as shown in Fig. 1. SEM demonstrated that these ultrafine Ni–P particles were distributed homogeneously on the support in Ni–P/SiO_2 and Ni–W–P/SiO_2 samples, as shown in Fig. 2.

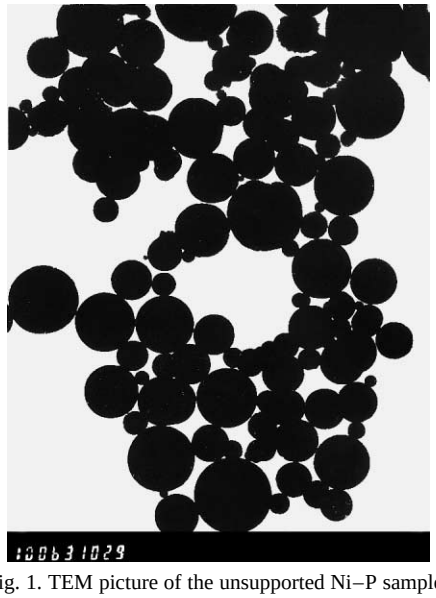

Fig. 1. TEM picture of the unsupported Ni–P sample.

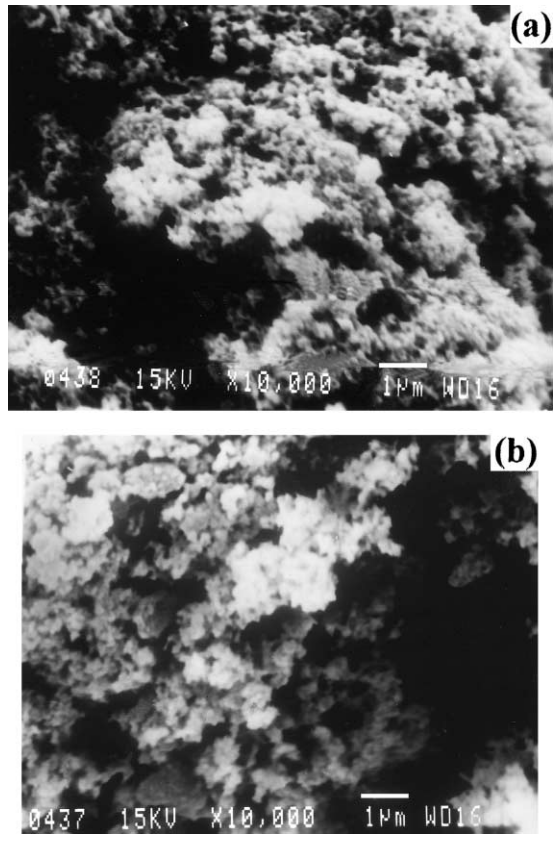

Fig. 2. SEM morphologies of (a) Ni–P/SiO_2 and (b) Ni–W–P/SiO_2 samples.

According to the XRD patterns, all the as-prepared Ni–P samples exhibited only one broad peak around $2\theta = 45°$, except for a broad peak at 22°, resulting from the amorphous SiO_2 support [15], indicating a typical amorphous structure as found in the Ni–P amorphous alloy obtained by the rapid quenching technique [16]. When these samples underwent a heating treatment at high temperature for 2.0 h in N_2 flow, various diffractional peaks indicative of the metallic Ni and crystalline Ni–P alloy phases, or sometimes the Ni–Al alloy phases in the case when Raney Ni–P was used, were observed on the XRD patterns, showing the occurrence of the crystallization process. The crystallization degree increased with the increase of the treatment temperature. A typical example was the crystallization of Ni–P/SiO_2 amorphous catalyst, as shown in Fig. 3.

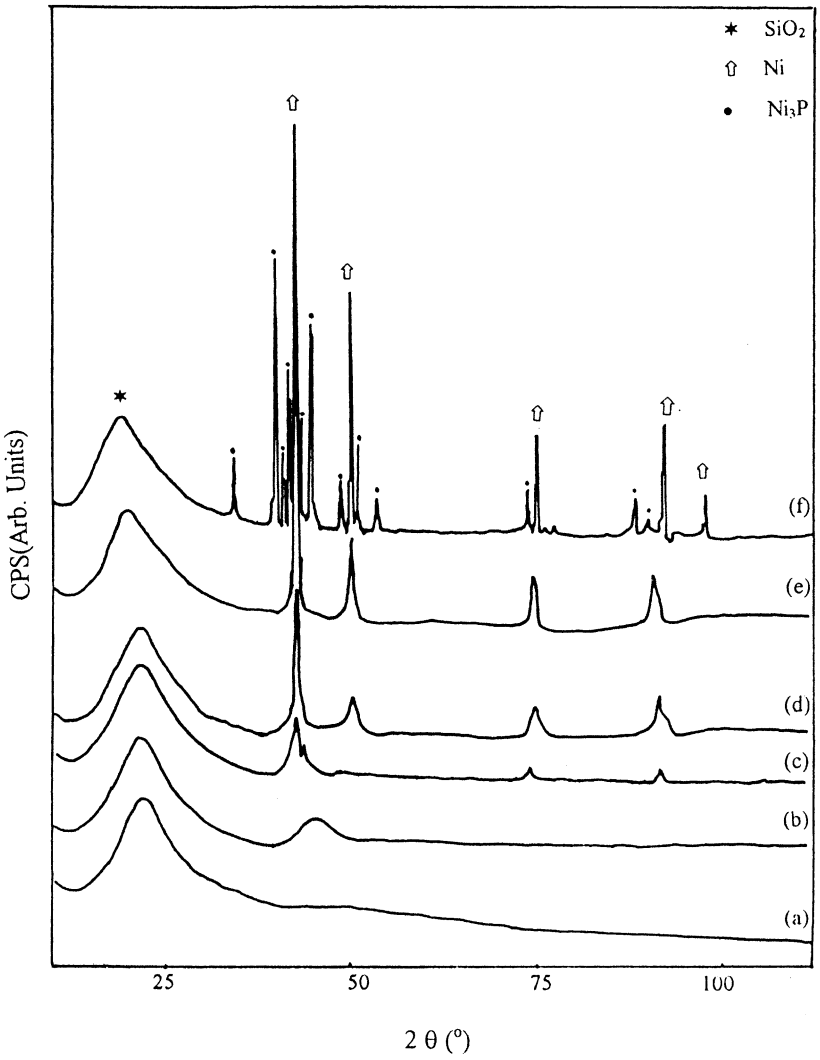

Fig. 3. XRD patterns of the fresh Ni–P/SiO_2 sample (a) and the Ni–P/SiO_2 sample pretreated in N_2 flow for 2.0 h at (b) 363, (c) 673, (d) 723, (e) 773 and (f) 873 K, respectively.

The crystallization of the Ni–P amorphous alloy at high temperature was further confirmed by extended X-ray absorption fine structure on Ni $\chi(k)k^3$ edge(EXAFS, BL-10B), from which the radial distribution functions (RDF) was obtained by fast Fourier transformation. For example, as shown in Fig. 4, the fresh Raney Ni–P sample exhibited only one broad peak around $R = 0.15–0.25$ nm, indicating that there was no long-range but only short-range ordering structure confined within the first-near-neighbor atom layer [17]. After being treated at 673 K for 2.0 h in N_2 flow, the peak around $R = 0.15–0.25$ nm became narrowed, and strengthened and two small additional peaks that appeared at longer range, showing the transformation from the amorphous structure to the well ordered crystalline structure [18]. Similar results were also obtained when other Ni–P samples were used, indicating that all the fresh samples were present in the amorphous structure regardless of the preparation methods, or the presence of silica support or the W-dopant. The above results also demonstrated that the all the Ni–P amorphous catalysts

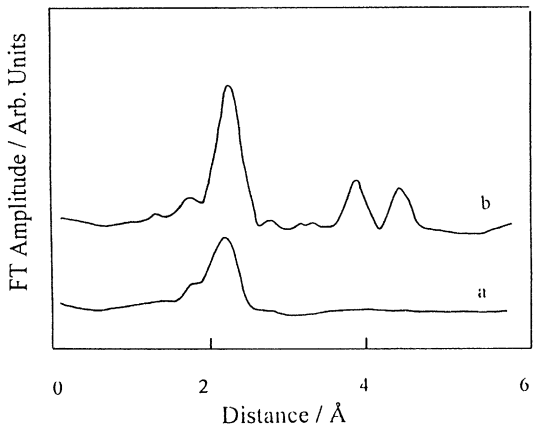

Fig. 4. RDF curves of (a) the fresh Raney Ni–P sample and (b) the Raney Ni–P sample after being treated 673 K for 2 h in N_2 flow.

would be crystallized spontaneously at high temperature, since the amorphous structure is thermodynamically metastable. However, DSC analysis revealed the promoting effects of the skeletal structure in Raney Ni–P, of the silica support in Ni–P/SiO_2 or of the W-dopant in Ni–W–P/SiO_2 on the thermal stability of amorphous structure, as shown in Fig. 5. This was mainly attributed to the increase in the dispersion degree of Ni–P alloy particles and the metal–support interaction [15,19].

The XPS spectra of the Ni–P/SiO_2 and Ni–W–P/SiO_2 amorphous catalysts, as shown in Fig. 6, revealed that nearly all the Ni and P species in the as-prepared catalysts were present in the metallic and alloying states corresponding to the binding energy (BE) values of 853.1 eV ($Ni_{2p_{3/2}}$) and 130.0 eV (P_{2p}), respectively. However, three kinds of W species were identified in W_{4f} level. Most were present in W^{+4} (BE = 32.8 eV), some were present in W^{+6} (BE = 35.7 eV), and very little were present in W^0 (BE = 30.5 eV). In comparison with the standard BE of metal Ni and pure red P [20], no significant BE shift of both the metallic Ni and alloying P was observed, regardless of the presence of trace of Al species, SiO_2 support or/and W-dopant. This indicates that electronic interaction between Ni and P in the Ni–P alloy was not important.

The compositions and the surface active areas (S_{Ni}) of the as-prepared samples were analyzed by ICP and the hydrogen chemisorption, respectively. As shown in Table 1, the ultrafine Ni–P sample had similar composition to the Ni–P/SiO_2. The addition of W-dopant caused an increase in the P content, since more $H_2PO_2^-$ was reduced by W^{+6} species. In contrast, Raney Ni–P had slightly lower P content. This was mainly due to the lower P content in the Ni–Al–P mother alloy limited by the eutectic point. After crystallization (treated at 673 K for 2 h in N_2 flow), the P content in the Raney Ni–P decreased slightly, which could be attributed to the partial sublimation of P species at high temperature [21]. Viewing the surface active area (S_{Ni}), one can see that both Raney Ni–P and Raney Ni exhibited very high S_{Ni} owing to their skeletal structure. After being crystallized, the S_{Ni} of Raney Ni–P decreased abruptly due to the gathering of the Ni–P alloy particles and the crush of the skeletal structure at high temperature. The ultrafine Ni–P catalyst had the lowest S_{Ni}, which was greatly enhanced in the presence of SiO_2 support, owing to the increase in the dispersion degree. Addition of little W-dopant into Ni–P/SiO_2 caused a slight decrease, since some surface active Ni atoms were covered by W oxides.

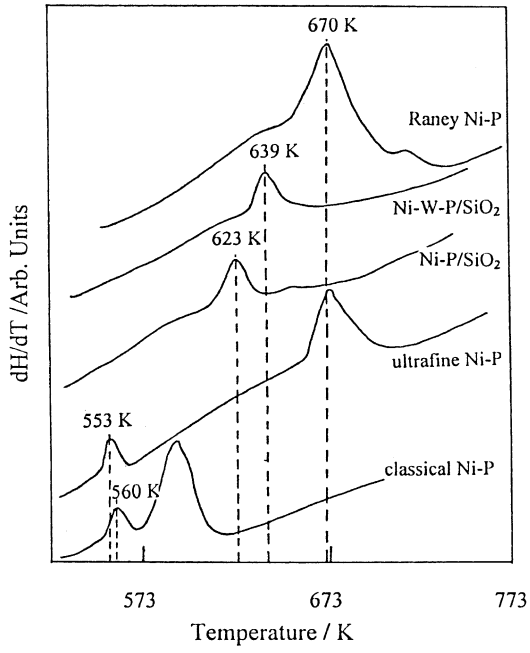

Fig. 5. DSC curves of various Ni–P amorphous catalysts.

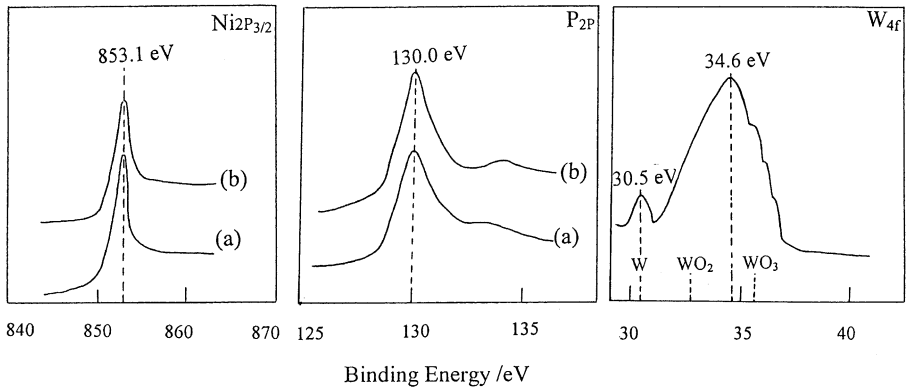

Fig. 6. XPS spectra of (a) the Ni–P/SiO_2 and (b) the Ni–W–P/SiO_2 amorphous catalysts.

The activities of various catalysts, both the TOF values and the H_2 uptake rates per gram Ni (R_{H_2}) are listed in Table 1. One can see that all the Ni–P amorphous catalysts exhibited higher TOF value than the Raney Ni catalyst. This was mainly attributed to the promoting effect of the unique amorphous structure and the alloying P. The promoting effect of the amorphous structure was supported by the fact that the crystallization of the Raney Ni–P (treated at 673 K for 2 h in N_2 flow) caused an abrupt decrease in both the TOF value and R_{H_2}. As the electronic effect was not significant according to the XPS spectra, one can conclude that the promoting effect was mainly resulted from the structural modification of the Ni active sites, such as the strong Ni–Ni interaction and the high unsaturated coordination of these Ni active sites [22]. The promoting effect of the alloying P could be clearly observed by comparing the TOF value of the crystallized Raney Ni–P with that of Raney Ni, but its mechanism was still not clear now, since no significant electronic interaction between Ni and P in the Ni–P alloy was observed by XPS spectra. The higher TOF value of Ni–W–P/SiO_2 sample than that of Ni–P/SiO_2 sample was attributed to the promoting effect of W-dopant. According to the XPS spectra, most of W species in the Ni–W–P/SiO_2 were present in the form of low-valent species (W^{+4} oxides). These W^{+4} oxides had strong affinity for the π-bond in benzene, leaving more Ni active sites for adsorbing hydrogen atoms [23]. Therefore, the hydrogenation activity increased, since the kinetic studies revealed that the benzene

Table 1
Structural characteristics and catalytic properties of the as-prepared catalysts
Reaction conditions: 1.0 g catalyst, 10 ml benzene, 40 ml EtOH; $T = 373$ K; $P_{H_2} = 1.0$ MPa.

Catalysts	Composition (at.%)	S_{Ni} (m^2/g)	TOF (10^{-3} s^{-1})	R_{H_2} (mmol/h g Ni)
Raney Ni–P	$Ni_{91}P_9$	38	24.2	52.7
Raney Ni–P(cryst)[a]	$Ni_{93}P_7$	15	12.5	12.8
Raney Ni	Ni	43	8.40	18.0
Ni–P/SiO_2[b]	$Ni_{86}P_{14}$	21	31.2	34.7
Ni–W–P/SiO_2[c]	$Ni_{81.5}W_{1.2}P_{17.3}$	19	42.4	40.8
Ultrafine Ni–P	$Ni_{86}P_{14}$	5.2	30.8	7.60

[a] Obtained by treating the fresh Raney Ni–P at 673 K for 2 h in N_2 flow.
[b] Ni loading = 11.5 wt%.
[c] Ni loading = 11.2 wt%; W/Ni molar ratio = 1.5%.

hydrogenation in liquid phase was the first order with respect to P_{H_2} and zero order with respect to benzene concentration under the present reaction conditions. Another promoting factor may be the increase of P content in the catalyst composition caused by the W-dopant, as shown in Table 1. Viewing the values of R_{H_2}, the following order was obtained: Raney Ni–P > Ni–W–P/SiO_2 > Ni–P/SiO_2 > Raney Ni > ultrafine Ni–P. The higher R_{H_2} of Raney Ni–P than that of Ni–W–P/SiO_2 was mainly attributed to its higher surface active area, owing to the skeletal structure. The higher R_{H_2} of Ni–W–P/SiO_2 than that of Ni–P/SiO_2 was mainly attributed to its higher TOF value, owing to the promoting effect of W-dopant. Since Raney Ni had the highest surface active area, the higher R_{H_2} values of Raney Ni–P, Ni–W–P/SiO_2 and Ni–P/SiO_2 amorphous catalysts than that of Raney Ni was mainly attributed to their higher TOF values. Although the ultrafine Ni–P amorphous catalyst exhibited much higher TOF value than Raney Ni, its R_{H_2} was slightly lower than that of Raney Ni due to its extremely lower surface active area.

4. Conclusions

In summary, the Ni–P amorphous catalysts exhibited much higher TOF values than Raney Ni in the liquid phase benzene hydrogenation, owing to the promoting effect of both the amorphous structure and the alloying P. These catalysts also exhibited higher R_{H_2} values than Raney Ni except for ultrafine Ni–P. W-dopant had a pronounced promoting effect on the activity of Ni–P amorphous catalyst, due to the affinity of W oxides at low valence (W^{+4} oxides). Generally, Ni–W–P/SiO_2 amorphous catalyst is more suitable for industrial processes because of its excellent activity and high thermal stability, as well as the simple procedure in preparation. It should be noted that the W-dopants had both an advantage and a disadvantage. On one hand, as discussed above, it could increase the TOF value and in turn, the R_{H_2} of the Ni–P amorphous catalyst. While on the other hand, a large concentration of W-dopant was detrimental to the activity because too many surface Ni atoms were covered by W species, similar to that found in Cr-doped Co–B amorphous alloy catalyst [24]. The optimum W/Ni molar ratio was determined in the range between 1.5% and 2.0%.

Acknowledgements

This work was supported by the National Natural Science Foundation of China. We also owe all our thanks to Shanghai Education Committee and Shanghai Science Foundation for their financial support.

References

[1] R.B. Moyes, P.B. Wells, Advances in Catalysis, Academic Press, New York, 1973.
[2] F.A. Dufau, F. Eschard, A.L. Haddad, C.H. Thonon, Chem. Age 17 (1966) 417.
[3] P. Fouilloux, Appl. Catal. 8 (1983) 1.
[4] A. Molnar, G.V. Smith, M. Bartok, Adv. Catal. 36 (1989) 329.
[5] I.G. Bulter, W. Kurz, J. Gillot, B. Fibre, Sci. Technol. 5 (1972) 243.
[6] H. Yamashita, M. Yoshikawa, T. Funabiki, S. Yoshida, J. Catal. 99 (1986) 375.
[7] S. Yoshida, H. Yamashita, T. Funabiki, T. Yonezawa, J. Chem. Soc., Faraday Trans. 1 80 (1984) 1435.
[8] J.F. Deng, H.X. Li, W.J. Wang, Catal. Today 51 (1999) 113.
[9] Y. Chen, Catal. Today 44 (1998) 3.
[10] J.F. Deng, J. Yang, S. Sheng, H. Chen, J. Catal. 150 (1994) 434.
[11] J.F. Deng, H. Chen, J. Mater. Sci. Lett. 12 (1993) 1508.
[12] H.X. Li, W. Dai, C. Shen, S. Zhou, J.F. Deng, Chem. Lett. (1997) 133.
[13] H.X. Li, Y. Xu, J.F. Deng, New J. Chem. 23 (1999) 1059.
[14] H.X. Li, M. Hui, Y. Xu, Chem. Lett. (2000) 1048.
[15] H.X. Li, W. Wang, H. Li, J.F. Deng, J. Catal. 194 (2000) 211.
[16] H. Yamashita, M. Yoshikawa, T. Funabiki, S. Yoshida, J. Chem. Soc., Faraday Trans. 1 82 (1986) 1771.
[17] J.A. Schwarz, C. Contescu, A. Contescu, Chem. Rev. 95 (1995) 477.
[18] H.X. Li, W. Wang, J.F. Deng, J. Catal. 191 (2000) 257.
[19] H.X. Li, H. Chen, S.Z. Dong, J. Yang, J.F. Deng, Appl. Surf. Sci. 125 (1998) 115.
[20] H. Li, H.X. Li, W. Dai, Z. Fang, J.F. Deng, Appl. Surf. Sci. 152 (1999) 25.
[21] F. Perlstein, R.F. Weightman, Electrochem. Technol. 6 (1968) 427.
[22] A. Baiker, Faraday Discuss. Chem. Soc. 87 (1989) 239.
[23] J. Volf, J. Pasek, Stud. Surf. Sci. Catal. 27 (1986) 105.
[24] H.X. Li, H. Li, M. Wang, Appl. Catal., accepted for publication.